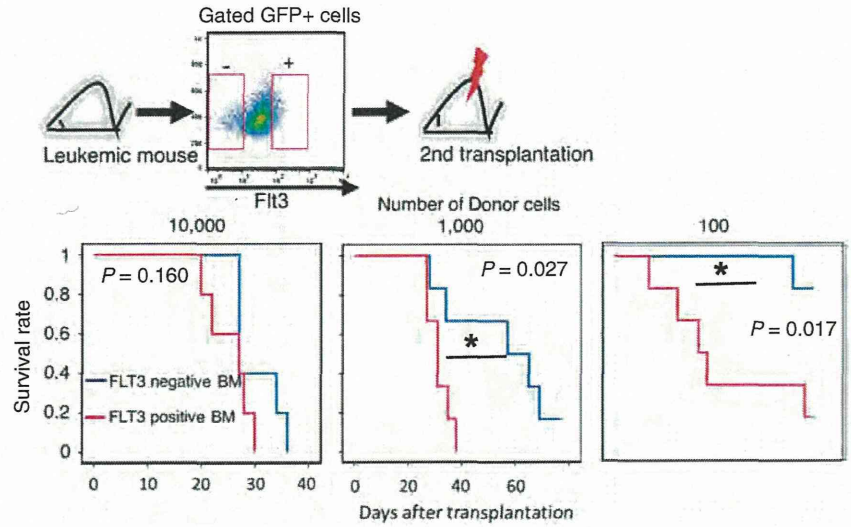

Figure 6. Upregulated FLT3 marks leukemia-initiating cells. (**a**) Survival of mice secondary transplanted with diluted numbers of FLT3-positive or -negative MLL–AF9/*Hes1*$^{-/-}$ AML cells prepared from the primary mice.

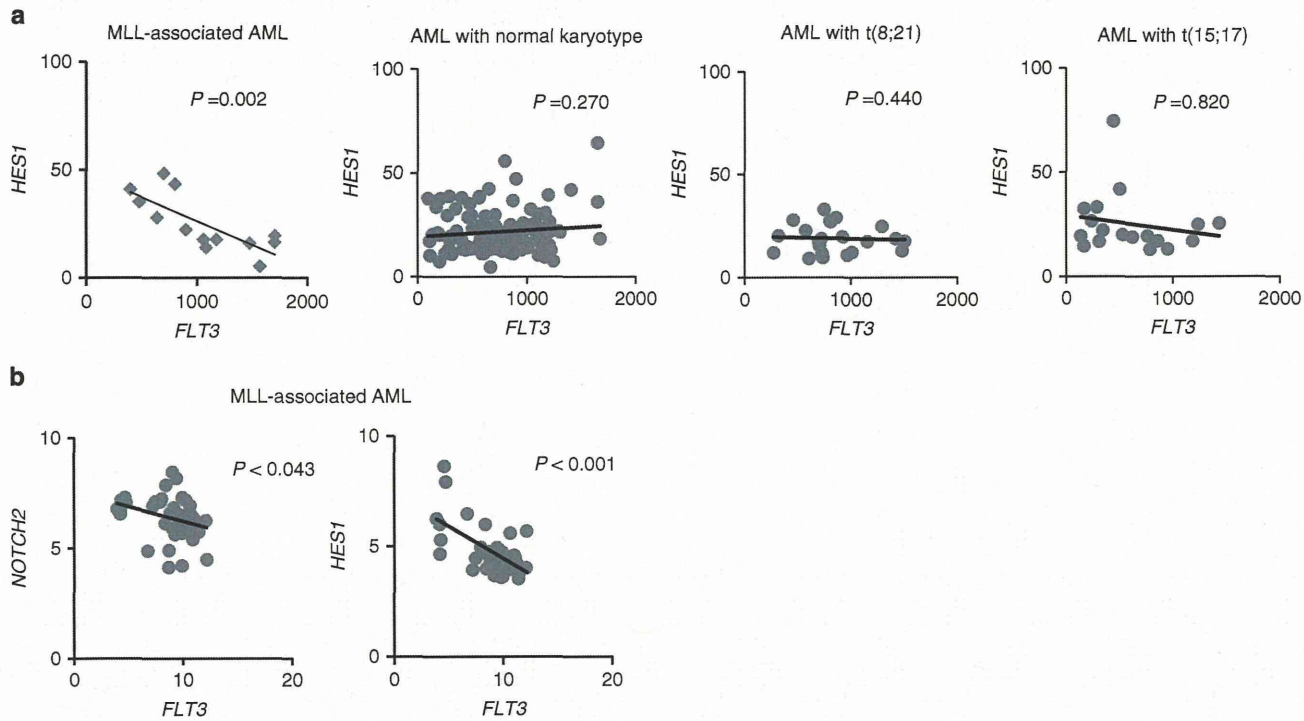

Figure 7. *FLT3* expression is negatively correlated with that of *HES1 in* MLL-related AML samples. (**a**) Re-analysis of the GSE1159 Gene Expression Omnibus database of AML tumor samples (deposited by Valk *et al.* [36]). Relative expression levels of *FLT3* and *HES1* in 13 MLL-related AML samples, 116 AML samples with normal karyotype, 18 AML samples with t(15;17) and 22 AML samples with t(8;21). (**b**) Reanalysis of the GSE19577 database (deposited by Pigazzi *et al.*[37]). Relative expression levels of *FLT3* and *NOTCH2*, and *FLT3* and *HES1* in 42 MLL-related AML samples.

samples, *FLT3* expression levels were negatively correlated with those of *HES1* and *NOTCH2*. In contrast, expression levels of *HES1* and *FLT3* showed no correlation in the MLL fusion-negative AML sub-cohort, although expression of *NOTCH2* and *FLT3* showed a negative correlation also in this population (Figure 7a and Supplementary Figure 5). We also assessed a different database derived from microarray analysis of 42 MLL-related AML samples (www.ncbi.nlm.nih.gov/geo, accession number GSE19577; ref. 37) and observed similar relationships between expression levels of *FLT3*, *NOTCH2* and *HES1* (Figure 7b).

A Notch agonist induces apoptosis of MLL–AF9-transduced cells dependently on Hes1

Flow cytometric analysis indicated that Notch2 is highly expressed on the surface of MLL–AF9-transduced cells, whereas other Notch

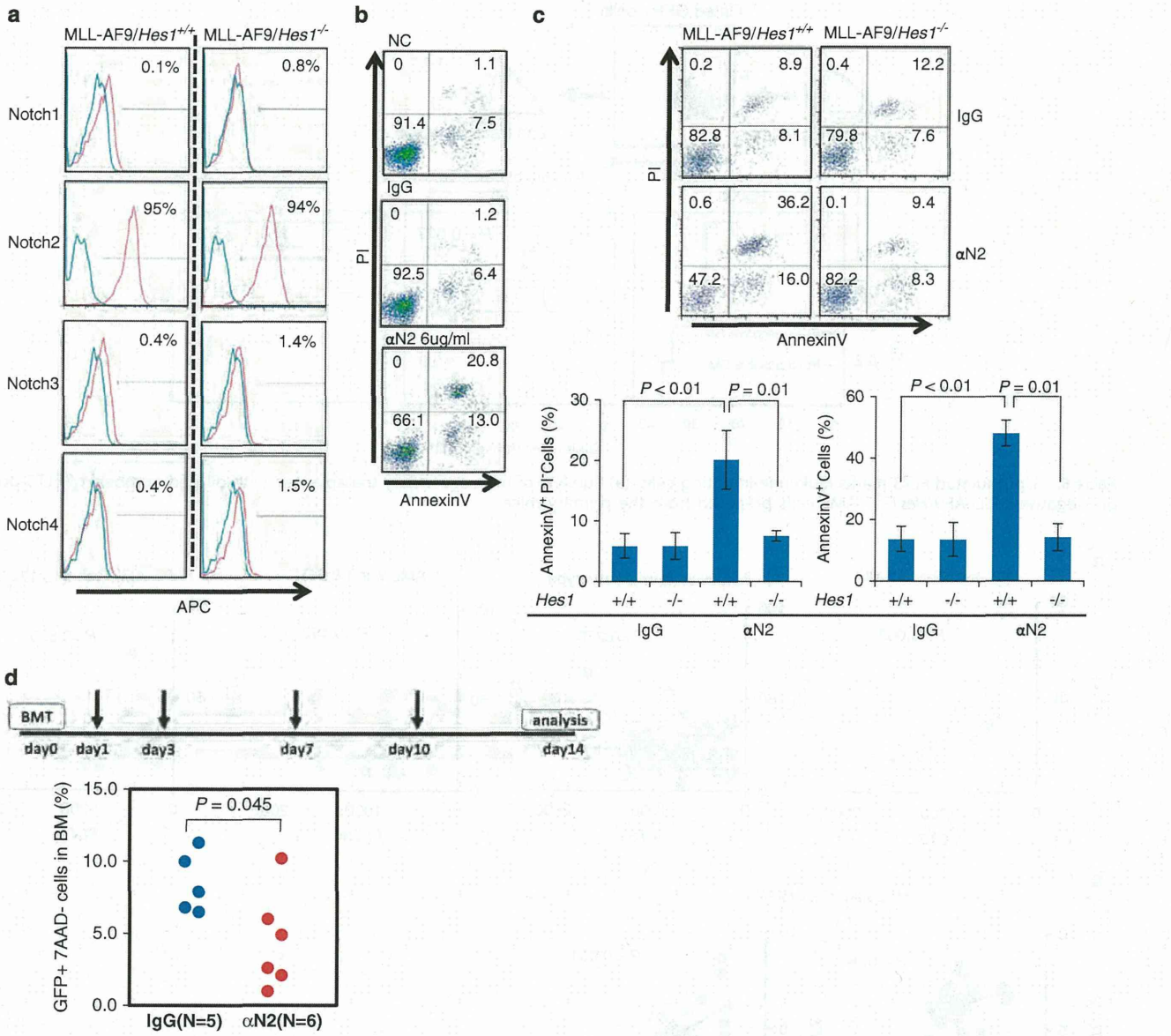

Figure 8. A Notch2 agonistic antibody induces apoptosis in MLL–AF9-transduced cells. (**a**) Cell-surface expression of Notch1–4 in MLL–AF9/*Hes1*$^{-/-}$ or MLL/AF9–*Hes1*$^{+/+}$ cells. Representative histograms are shown from three independent experiments. (**b**) Apoptosis of MLL–AF9 leukemic cells following treatment with anti-Notch2 agonistic antibody. Shown is a representative result from three independent experiments. (**c**) Apoptosis of MLL–AF9-transduced cells following Notch2 stimulation requires Hes1. (Left) A representative flow cytometric pattern from three independent experiments. (Right) Summary of three independent experiments. (**d**)Therapeutic AML mouse model using an agonistic anti-Notch2 antibody. Hamster anti-mouse Notch2 (HMN2–29, 100 μg/mouse) or hamster immunoglobulin-G (IgG; 100 μg/mouse) was injected on days 1, 3, 7 and 10 after transplantation of MLL–AF9/*Hes1*$^{+/+}$-transduced cells. The engraftment ratio, which is shown by the GFP-positive cell ratio in bone marrow, was measured by flow cytometry at day 14 after transplantation. αN2, anti-Notch2 antibody.

family receptors were either undetectable or detectable at low levels (Figure 8a). Thus, to evaluate the effect of Notch2 signaling we treated MLL–AF9-transduced cells with a hamster anti-mouse Notch2 agonistic antibody or control immunoglobulin-G.[38] Notch2 antibody treatment significantly induced apoptosis in MLL–AF9 cells compared with immunoglobulin-G-treated cells (Figure 8b), which was abrogated in a *Hes1*-null background (Figure 8c). This effect was also blocked when MLL–AF9-transduced cells were treated with the Notch2 agonistic antibody in the presence of a γ-secretase inhibitor, DAPT, which inhibits Notch signaling (Supplementary Figure 6), indicating that apoptosis requires Notch cleavage. Furthermore we performed a therapeutic animal model experiment using a Notch2 agonistic antibody, and found that the antibody was also effective *in vivo*. The frequencies of leukemic cells, which is shown by the GFP-positive cell ratio in bone marrow were significantly reduced in mice treated with the Notch2 agonistic antibody compared with immunoglobulin-G (Figure 8d).

DISCUSSION

AML is characterized by clonal expansion of myeloid progenitor cells in bone marrow. *MLL* fusion genes are detected in ~5% of AML patients and have an unfavorable impact on the prognosis.

Development of new treatment strategies requires better understanding of the molecular pathogenesis of *MLL*-related AML.

In hematopoietic malignancies, Notch signaling has both tumor-promoting and -suppressive roles depending on context. Although the significance of Notch signaling in myeloid malignancies remains controversial, our results, together with previous reports,[23,24] strongly suggest that Notch signaling physiologically suppresses development of a broad range of myeloid leukemias, including AML. In our model, Notch stimulation resulted in the growth suppression of AML cells, implying that Notch agonistic agents could serve as treatment modalities, as previously suggested by others.[24] Notch signal inhibitors, such as γ-secretase inhibitors, have been developed as drugs for T-ALL.[39,40] If either Notch-activating or Notch-suppressive drugs prove effective, accurate diagnosis would be critical, making it necessary to identify new biomarkers that could precisely predict indications to each medicine.

The dichotomous functions of Notch signaling may result from differences in downstream targets. The proto-oncogene *MYC* was shown to be a direct transcriptional target of Notch–RBPJ and contribute to tumor progression in T-ALL,[41] and Hes1 has been demonstrated to have a major role in downstream Notch signaling for T-ALL promotion.[42] Nevertheless, Hes1 was subsequently suggested to be a downstream mediator of Notch signaling in suppressing B-cell ALL cell growth.[19] Although several groups have indicated possible tumor-suppressive function of Notch–Hes1 axis, also in AML, the work described here is the first genetic evidence showing that Hes1 actually has an essential role as a tumor suppressor downstream to Notch signaling.

The observation that Hes1 is activated in varying contexts implies that distinct downstream regulatory networks are utilized to promote or suppress a wide range of hematologic malignancies. For T-ALL development, repression of the tumor suppressors CYLD and PTEN is proposed to mediate the Notch–RBPJ–Hes1 pathway,[43,44] while in a very different context, poly ADP-ribose polymerase1 is activated by interaction with Hes1 and functions to induce apoptosis of B-ALL cells.[19]

We identified FLT3 downregulation as a target of Hes1 in suppressing AML development. Activating mutations in *FLT3* gene are seen in up to 30% of AML patients.[45] In particular, FLT3-internal tandem duplication mutations are associated with poor survival when AML patients are treated with standard chemotherapy. In addition, recent studies indicate that ~10–15% of AML patients display high expression of wild-type *FLT3*.[46] High *FLT3* expression has a negative impact on overall and event-free survival in cytogenetically normal AML patients lacking *FLT3* mutations.[47] This fact might be relevant to the enhanced AML development and increased *FLT3* expression we report here in a mouse model: in AML seen in patients or mouse models, increased tyrosine kinase activity is likely to be a key. Although FLT3 inhibitors have been developed for clinical use,[48] it is not known whether high FLT3 levels could serve as a biomarker to predict efficacy or resistance to those inhibitors.

Expression levels of *FLT3* and *HES1* were negatively correlated only in *MLL* fusion-associated AML, as determined by analysis of public databases, implying that FLT3 upregulation by the Notch–RBPJ–Hes1 pathway is confined to just MLL–AF9-induced AML, rather than universal to AML of diverse molecular backgrounds or confined to just MLL–AF9-induced AML. Nevertheless, Lobry *et al.*[23] reported that Notch signaling has a tumor suppressive role in a broad range of AML cells. Thus, whether distinct effectors operate downstream of *Notch* in MLL fusion-positive and -negative AMLs needs to be clarified. In this regard, our microarray analysis of *Hes1*-deficient AML cells identified, in addition to *Flt3*, several other candidate genes such as *Eya1*, *Six1* and *Jun* (data not shown). Eya1 and Six1 are known to be direct transcriptional targets of MLL–AF9.[49] Eya1 overexpression immortalizes hematopoietic progenitor cells and its co-transduction with Six1 potentiates Eya1's transforming capacity.[49] Jun, an important component of the JNK pathway, has not been described as a direct MLL–AF9 target. These data suggest that the Notch–RBPJ–Hes1 axis suppresses MLL–AF9 leukemia by modulating direct and indirect targets of MLL–AF9.

In summary, we have demonstrated that the Notch–RBPJ–Hes1 axis functions as a tumor suppressor in AML, probably via, at least in part, repression of FLT3. Our results provide insight into AML pathogenesis and may suggest novel therapeutic approaches to the disease.

CONFLICT OF INTEREST

The authors declare no conflict of interest.

ACKNOWLEDGEMENTS

We thank Drs T Machino and T Enami (University of Tsukuba) for discussion; Drs A Yokoyama (Kyoto University), H Nakauchi (University of Tokyo/Stanford University), and, M Onodera (National Research Institute for Child Health and Development) for vectors. We also thank T Takahashi for mouse experiments. We are also grateful to Kyowa Hakko Kirin Co., Ltd. for KRN383. This work was supported by Grants-in-Aid for Scientific Research (KAKENHI) from the Ministry of Education, Culture, Sports, Science and Technology of Japan (25860778 to TK; 25461407 to MS-Y; and 25112703, 24390241, 23118503 and 22130002 to SC) and supported by the Sagawa Cancer Foundation, the Naito Foundation, the Kato Memorial Bioscience Foundation and the YASUDA Medical Foundation to MS-Y.

REFERENCES

1 Artavanis-Tsakonas S, Rand MD, Lake RJ. Notch signaling: cell fate control and signal integration in development. *Science* 1999; **284**: 770–776.
2 De Strooper B, Annaert W, Cupers P, Saftig P, Craessaerts K, Mumm JS *et al.* A presenilin-1-dependent gamma-secretase-like protease mediates release of Notch intracellular domain. *Nature* 1999; **398**: 518–522.
3 Kageyama R, Ohtsuka T, Tomita K. The bHLH gene Hes1 regulates differentiation of multiple cell types. *Mol Cells* 2000; **10**: 1–7.
4 Oswald F, Tauber B, Dobner T, Bourteele S, Kostezka U, Adler G *et al.* p300 acts as a transcriptional coactivator for mammalian Notch-1. *Mol Cell Biol* 2001; **21**: 7761–7774.
5 Bigas A, Espinosa L. Hematopoietic stem cells: to be or Notch to be. *Blood* 2012; **119**: 3226–3235.
6 Grbavec D, Stifani S. Molecular interaction between TLE1 and the carboxyl-terminal domain of HES-1 containing the WRPW motif. *Biochem Biophys Res Commun* 1996; **223**: 701–705.
7 Ito T, Udaka N, Okudela K, Yazawa T, Kitamura H. Mechanisms of neuroendocrine differentiation in pulmonary neuroendocrine cells and small cell carcinoma. *Endocr Pathol* 2003; **14**: 133–139.
8 Ito T, Udaka N, Yazawa T, Okudela K, Hayashi H, Sudo T *et al.* Basic helix-loop-helix transcription factors regulate the neuroendocrine differentiation of fetal mouse pulmonary epithelium. *Development* 2000; **127**: 3913–3921.
9 Weng AP, Ferrando AA, Lee W, Morris JP 4th, Silverman LB, Sanchez-Irizarry C *et al.* Activating mutations of NOTCH1 in human T cell acute lymphoblastic leukemia. *Science* 2004; **306**: 269–271.
10 Suzuki T, Chiba S. Notch signaling in hematopoietic stem cells. *Int J Hematol* 2005; **82**: 285–294.
11 Radtke F, Wilson A, Stark G, Bauer M, van Meerwijk J, MacDonald HR *et al.* Deficient T cell fate specification in mice with an induced inactivation of Notch1. *Immunity* 1999; **10**: 547–558.
12 Puente XS, Pinyol M, Quesada V, Conde L, Ordonez GR, Villamor N *et al.* Whole-genome sequencing identifies recurrent mutations in chronic lymphocytic leukaemia. *Nature* 2011; **475**: 101–105.
13 Kridel R, Meissner B, Rogic S, Boyle M, Telenius A, Woolcock B *et al.* Whole transcriptome sequencing reveals recurrent NOTCH1 mutations in mantle cell lymphoma. *Blood* 2012; **119**: 1963–1971.
14 Lee SY, Kumano K, Nakazaki K, Sanada M, Matsumoto A, Yamamoto G *et al.* Gain-of-function mutations and copy number increases of Notch2 in diffuse large B-cell lymphoma. *Cancer Sci* 2009; **100**: 920–926.
15 Kiel MJ, Velusamy T, Betz BL, Zhao L, Weigelin HG, Chiang MY *et al.* Whole-genome sequencing identifies recurrent somatic NOTCH2 mutations in splenic marginal zone lymphoma. *J Exp Med* 2012; **209**: 1553–1565.

16 Robinson DR, Kalyana-Sundaram S, Wu YM, Shankar S, Cao X, Ateeq B *et al.* Functionally recurrent rearrangements of the MAST kinase and Notch gene families in breast cancer. *Nat Med* 2011; **17**: 1646–1651.
17 Nicolas M, Wolfer A, Raj K, Kummer JA, Mill P, van Noort M *et al.* Notch1 functions as a tumor suppressor in mouse skin. *Nat Genet* 2003; **33**: 416–421.
18 Yan M, Callahan CA, Beyer JC, Allamneni KP, Zhang G, Ridgway JB *et al.* Chronic DLL4 blockade induces vascular neoplasms. *Nature* 2010; **463**: E6–E7.
19 Kannan S, Fang W, Song G, Mullighan CG, Hammitt R, McMurray J *et al.* Notch/HES1-mediated PARP1 activation: a cell type-specific mechanism for tumor suppression. *Blood* 2011; **117**: 2891–2900.
20 Nakahara F, Sakata-Yanagimoto M, Komeno Y, Kato N, Uchida T, Haraguchi K *et al.* Hes1 immortalizes committed progenitors and plays a role in blast crisis transition in chronic myelogenous leukemia. *Blood* 2010; **115**: 2872–2881.
21 Ito T, Kwon HY, Zimdahl B, Congdon KL, Blum J, Lento WE *et al.* Regulation of myeloid leukaemia by the cell-fate determinant Musashi. *Nature* 2010; **466**: 765–768.
22 Klinakis A, Lobry C, Abdel-Wahab O, Oh P, Haeno H, Buonamici S *et al.* A novel tumour-suppressor function for the Notch pathway in myeloid leukaemia. *Nature* 2011; **473**: 230–233.
23 Lobry C, Ntziachristos P, Ndiaye-Lobry D, Oh P, Cimmino L, Zhu N *et al.* Notch pathway activation targets AML-initiating cell homeostasis and differentiation. *J Exp Med* 2013; **210**: 301–319.
24 Kannan S, Sutphin RM, Hall MG, Golfman LS, Fang W, Nolo RM *et al.* Notch activation inhibits AML growth and survival: a potential therapeutic approach. *J Exp Med* 2013; **210**: 321–337.
25 Han H, Tanigaki K, Yamamoto N, Kuroda K, Yoshimoto M, Nakahata T *et al.* Inducible gene knockout of transcription factor recombination signal binding protein-J reveals its essential role in T versus B lineage decision. *Int Immunol* 2002; **14**: 637–645.
26 Tanigaki K, Han H, Yamamoto N, Tashiro K, Ikegawa M, Kuroda K *et al.* Notch-RBP-J signaling is involved in cell fate determination of marginal zone B cells. *Nat Immunol* 2002; **3**: 443–450.
27 Guiu J, Shimizu R, D'Altri T, Fraser ST, Hatakeyama J, Bresnick EH *et al.* Hes repressors are essential regulators of hematopoietic stem cell development downstream of Notch signaling. *J Exp Med* 2013; **210**: 71–84.
28 Tomita K, Ishibashi M, Nakahara K, Ang SL, Nakanishi S, Guillemot F *et al.* Mammalian hairy and Enhancer of split homolog 1 regulates differentiation of retinal neurons and is essential for eye morphogenesis. *Neuron* 1996; **16**: 723–734.
29 Somervaille TC, Cleary ML. Identification and characterization of leukemia stem cells in murine MLL-AF9 acute myeloid leukemia. *Cancer Cell* 2006; **10**: 257–268.
30 Sang L, Coller HA, Roberts JM. Control of the reversibility of cellular quiescence by the transcriptional repressor HES1. *Science* 2008; **321**: 1095–1100.
31 McLarren KW, Theriault FM, Stifani S. Association with the nuclear matrix and interaction with Groucho and RUNX proteins regulate the transcription repression activity of the basic helix loop helix factor Hes1. *J Biol Chem* 2001; **276**: 1578–1584.
32 Kang HJ, Lee JW, Kho SH, Kim MJ, Seo YJ, Kim H *et al.* High transcript level of FLT3 associated with high risk of relapse in pediatric acute myeloid leukemia. *J Korean Med Sci* 2010; **25**: 841–845.
33 Ozeki K, Kiyoi H, Hirose Y, Iwai M, Ninomiya M, Kodera Y *et al.* Biologic and clinical significance of the FLT3 transcript level in acute myeloid leukemia. *Blood* 2004; **103**: 1901–1908.
34 Hayakawa F, Towatari M, Kiyoi H, Tanimoto M, Kitamura T, Saito H *et al.* Tandem-duplicated Flt3 constitutively activates STAT5 and MAP kinase and introduces autonomous cell growth in IL-3-dependent cell lines. *Oncogene* 2000; **19**: 624–631.
35 Komeno Y, Kurokawa M, Imai Y, Takeshita M, Matsumura T, Kubo K *et al.* Identification of Ki23819, a highly potent inhibitor of kinase activity of mutant FLT3 receptor tyrosine kinase. *Leukemia* 2005; **19**: 930–935.
36 Valk PJ, Verhaak RG, Beijen MA, Erpelinck CA, Barjesteh van Waalwijk van Doorn-Khosrovani S, Boer JM *et al.* Prognostically useful gene-expression profiles in acute myeloid leukemia. *N Engl J Med* 2004; **350**: 1617–1628.
37 Pigazzi M, Masetti R, Bresolin S, Beghin A, Di Meglio A, Gelain S *et al.* MLL partner genes drive distinct gene expression profiles and genomic alterations in pediatric acute myeloid leukemia: an AIEOP study. *Leukemia* 2011; **25**: 560–563.
38 Moriyama Y, Sekine C, Koyanagi A, Koyama N, Ogata H, Chiba S *et al.* Delta-like 1 is essential for the maintenance of marginal zone B cells in normal mice but not in autoimmune mice. *Int Immunol* 2008; **20**: 763–773.
39 Paganin M, Ferrando A. Molecular pathogenesis and targeted therapies for NOTCH1-induced T-cell acute lymphoblastic leukemia. *Blood Rev* 2011; **25**: 83–90.
40 Samon JB, Castillo-Martin M, Hadler M, Ambesi-Impiobato A, Paietta E, Racevskis J *et al.* Preclinical analysis of the gamma-secretase inhibitor PF-03084014 in combination with glucocorticoids in T-cell acute lymphoblastic leukemia. *Mol Cancer Ther* 2012; **11**: 1565–1575.
41 Weng AP, Millholland JM, Yashiro-Ohtani Y, Arcangeli ML, Lau A, Wai C *et al.* c-Myc is an important direct target of Notch1 in T-cell acute lymphoblastic leukemia/lymphoma. *Genes Dev* 2006; **20**: 2096–2109.
42 Wendorff AA, Koch U, Wunderlich FT, Wirth S, Dubey C, Brüning JC *et al.* Hes1 is a critical but context-dependent mediator of canonical notch signaling in lymphocyte development and transformation. *Immunity* 2010; **33**: 671–684.
43 Espinosa L, Cathelin S, D'Altri T, Trimarchi T, Statnikov A, Guiu J *et al.* The Notch/Hes1 pathway sustains NF-kappaB activation through CYLD repression in T cell leukemia. *Cancer Cell* 2010; **18**: 268–281.
44 Palomero T, Sulis ML, Cortina M, Real PJ, Barnes K, Ciofani M *et al.* Mutational loss of PTEN induces resistance to NOTCH1 inhibition in T-cell leukemia. *Nat Med* 2007; **13**: 1203–1210.
45 Frohling S, Schlenk RF, Breitruck J, Benner A, Kreitmeier S, Tobis K *et al.* Prognostic significance of activating FLT3 mutations in younger adults (16 to 60 years) with acute myeloid leukemia and normal cytogenetics: a study of the AML Study Group Ulm. *Blood* 2002; **100**: 4372–4380.
46 Riccioni R, Pelosi E, Riti V, Castelli G, Lo-Coco F, Testa U. Immunophenotypic features of acute myeloid leukaemia patients exhibiting high FLT3 expression not associated with mutations. *Br J Haematol* 2011; **153**: 33–42.
47 Kuchenbauer F, Kern W, Schoch C, Kohlmann A, Hiddemann W, Haferlach T *et al.* Detailed analysis of FLT3 expression levels in acute myeloid leukemia. *Haematologica* 2005; **90**: 1617–1625.
48 Kindler T, Lipka DB, Fischer T. FLT3 as a therapeutic target in AML: still challenging after all these years. *Blood* 2010; **116**: 5089–5102.
49 Wang QF, Wu G, Mi S, He F, Wu J, Dong J *et al.* MLL fusion proteins preferentially regulate a subset of wild-type MLL target genes in the leukemic genome. *Blood* 2011; **117**: 6895–6905.

Supplementary Information accompanies this paper on the Leukemia website (http://www.nature.com/leu)

OPEN ACCESS Freely available online

PLOS | ONE

Detection of the G17V RHOA Mutation in Angioimmunoblastic T-Cell Lymphoma and Related Lymphomas Using Quantitative Allele-Specific PCR

**Rie Nakamoto-Matsubara[1], Mamiko Sakata-Yanagimoto[1,2,3], Terukazu Enami[1], Kenichi Yoshida[4], Shintaro Yanagimoto[5], Yusuke Shiozawa[4], Tohru Nanmoku[6], Kaishi Satomi[7], Hideharu Muto[1,2,3], Naoshi Obara[1,2,3], Takayasu Kato[1,2,3,8], Naoki Kurita[1,2,3], Yasuhisa Yokoyama[1,2,3], Koji Izutsu[9,10], Yasunori Ota[11], Masashi Sanada[4], Seiichi Shimizu[3,12], Takuya Komeno[3,13], Yuji Sato[14], Takayoshi Ito[15], Issay Kitabayashi[16], Kengo Takeuchi[17], Naoya Nakamura[18], Seishi Ogawa[4], Shigeru Chiba[1,2,3,8]*

1 Department of Hematology, Graduate School of Comprehensive Human Sciences, University of Tsukuba, Tsukuba, Ibaraki, Japan, **2** Department of Hematology, Faculty of Medicine, University of Tsukuba, Tsukuba, Ibaraki, Japan, **3** Department of Hematology, University of Tsukuba Hospital, Tsukuba, Ibaraki, Japan, **4** Department of Pathology and Tumor Biology, Graduate School of Medicine, Kyoto University, Sakyo-ku, Kyoto, Japan, **5** Division for Health Service Promotion, The University of Tokyo, Bunkyo-ku, Tokyo, Japan, **6** Department of Clinical Laboratory, University of Tsukuba Hospital, Tsukuba, Ibaraki, Japan, **7** Department of Pathology, University of Tsukuba Hospital, Tsukuba, Ibaraki, Japan, **8** Life Science Center, Tsukuba Advanced Research Center, University of Tsukuba, Tsukuba, Ibaraki, Japan, **9** Department of Hematology, Toranomon Hospital, Minato-ku, Tokyo, Japan, **10** Okinaka Memorial Institute for Medical Research, Minato-ku, Tokyo, Japan, **11** Department of Pathology, Toranomon Hospital, Minato-ku, Tokyo, Japan, **12** Department of Hematology, Tsuchiura Kyodo General Hospital, Tsuchiura, Ibaraki, Japan, **13** Department of Hematology, Mito Medical Center, National Hospital Organization, Ibaraki-machi, Ibaraki, Japan, **14** Department of Hematology, Tsukuba Memorial Hospital, Tsukuba, Ibaraki, Japan, **15** Department of Hematology, JA Toride Medical Center, Toride, Ibaraki, Japan, **16** Division of Hematological Malignancy, National Cancer Center Research Institute, Chuo-ku, Tokyo, Japan, **17** Pathology Project for Molecular Targets, The Cancer Institute, Japanese Foundation for Cancer Research, Koto-ku, Tokyo, Japan, **18** Department of Pathology, Tokai University School of Medicine, Isehara, Kanagawa, Japan

Abstract

Angioimmunoblastic T-cell lymphoma (AITL) and peripheral T-cell lymphoma, not otherwise specified (PTCL-NOS) are subtypes of T-cell lymphoma. Due to low tumor cell content and substantial reactive cell infiltration, these lymphomas are sometimes mistaken for other types of lymphomas or even non-neoplastic diseases. In addition, a significant proportion of PTCL-NOS cases reportedly exhibit features of AITL (AITL-like PTCL-NOS). Thus disagreement is common in distinguishing between AITL and PTCL-NOS. Using whole-exome and subsequent targeted sequencing, we recently identified G17V *RHOA* mutations in 60–70% of AITL and AITL-like PTCL-NOS cases but not in other hematologic cancers, including other T-cell malignancies. Here, we establish a sensitive detection method for the G17V *RHOA* mutation using a quantitative allele-specific polymerase chain reaction (qAS-PCR) assay. Mutated allele frequencies deduced from this approach were highly correlated with those determined by deep sequencing. This method could serve as a novel diagnostic tool for 60–70% of AITL and AITL-like PTCL-NOS.

Citation: Nakamoto-Matsubara R, Sakata-Yanagimoto M, Enami T, Yoshida K, Yanagimoto S, et al. (2014) Detection of the G17V RHOA Mutation in Angioimmunoblastic T-Cell Lymphoma and Related Lymphomas Using Quantitative Allele-Specific PCR. PLoS ONE 9(10): e109714. doi:10.1371/journal.pone.0109714

Editor: Kristy L. Richards, University of North Carolina at Chapel Hill, United States of America

Received March 27, 2014; **Accepted** September 4, 2014; **Published** October 13, 2014

Data Availability: The authors confirm that all data underlying the findings are fully available without restriction. All relevant data are within the paper and its Supporting Information files.

Funding: This work was supported by Grants-in-Aid for Scientific Research (KAKENHI) (24390241, 23659482, 23118503, and 22130002 to S.C.; 25461407 to M.S.-Y.), and the Adaptable and Seamless Technology Transfer Program through target-driven R and D (A-STEP) to M.S.-Y. from the Ministry of Education, Culture, Sports, Science and Technology of Japan. This work was also supported by the Mochida Memorial Foundation for Medical and Pharmaceutical Research, and the Uehara Memorial Foundation to M.S.-Y. The funders had no role in study design, data collection and analysis, decision to publish, or preparation of the manuscript.

Competing Interests: The authors have declared that no competing interests exist.

* Email: schiba-tky@umin.net

Introduction

Based on the classification proposed by the World Health Organization (WHO), Angioimmunoblastic T-cell lymphoma (AITL) is a distinct subtype of T-cell lymphoma that accounts for 20% of peripheral T-cell lymphoma cases [1]. AITL is characterized by generalized lymphadenopathy, hyperglobulinemia, and autoimmune-like manifestations [1,2]. Pathologic examination of AITL tumors reveals polymorphous infiltration of reactive cells, including endothelial venules and follicular dendritic cells [3,4]. Based on gene expression profiling and immunohistochemical staining, the normal counterparts of AITL tumor cells are proposed to be follicular helper T cells (TFHs) [5]. Peripheral T-cell lymphoma, not otherwise specified (PTCL-NOS) is a more heterogenous type of lymphoma, one that shows variation even in CD4 and CD8 expression. Some PTCL-NOS cases share features of AITL, such as immunohistochemical

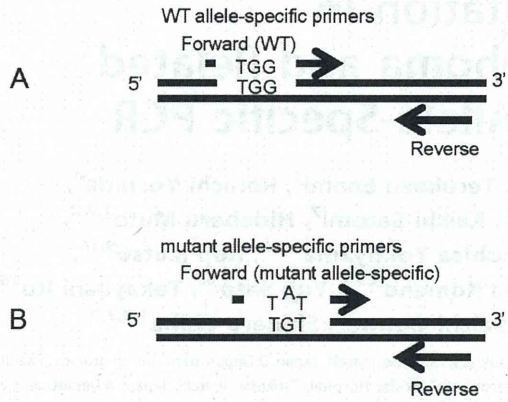

Figure 1. Design of primers used in the study. A WT allele-specific primer forward primer (Upper), a mutant allele-specific forward primer (Lower), and a common primer were designed. The 3′ end of the forward mutant primer was specific to the mutant site (G to T) and an internal mismatch at the second nucleotide from 3′ end (G to A) was introduced to improve specificity.
doi:10.1371/journal.pone.0109714.g001

staining patterns resembling those seen in AITL (AITL-like PTCL-NOS) [6].

Expertise is required to diagnose AITL and PTCL-NOS because generally low tumor cell content obscures the neoplastic nature of some cases, and large reactive B-cells are often confused with tumor cells [7]. Clonal rearrangement of the T-cell receptor gene is undetectable in 10–25% of AITL cases due to low tumor cell frequency [1]. In addition, clonal growth of Epstein-Bar virus-infected B-cells is not uncommon in these kinds of cancers, causing detection of clonal immunoglobulin gene rearrangement in 20% of these case. [1].

Mutations in *TET2, IDH2*, and *DNMT3A* are frequently seen in AITL and AITL-like PTCL-NOS [8,9], although these mutations are also common to various myeloid malignancies [10,11]. We and others reported a large cohort of AITL and PTCL-NOS patients revealing that the G17V *RHOA* mutation was highly specific to AITL and AITL-like PTCL-NOS and very frequent (seen in 60–70% of cases) in these T-cell lymphomas [12,13]. This observation suggests that detection of the G17V *RHOA* mutation could serve as a new diagnostic tool to discriminate these lymphomas from other diseases. One difficulty, however, is that *RHOA* mutation allele frequencies in these lymphomas are generally as low as <0.2 or often <0.1, reflecting low tumor cell content. Therefore, diagnosis of these conditions requires development of sensitive and cost-efficient methods that are as accurate as deep sequencing, which is expensive and not commonly used in most clinical testing facilities.

To meet this need, we developed a quantitative allele-specific polymerase chain reaction (qAS-PCR) method that sensitively detects the G17V *RHOA* mutation in a highly accurate manner. This assay should provide a realistic way to conduct laboratory testing to diagnose AITL and AITL-like PTCL-NOS.

Materials and Methods

Primer design

We designed two forward primers that discriminate wild-type (WT) from G17V *RHOA* for use with one common reverse primer. The mutant forward primer was designed using a previously described algorithm [14]. The 3′ end is specific to the mutant site and an internal mismatch at the second nucleotide from the 3′ end was introduced to improve specificity (Figure 1 and Table 1). We performed local alignment analysis using the BLAST program (http://www.ncbi.nlm.nih.gov/tools/primer-blast/) to confirm primer specificity.

Preparation of plasmids containing WT and mutant cDNA and standard curve generation

WT or G17V mutant *RHOA* cDNA was subcloned into pBluescript (pBS/wtRHOA or pBS/mutRHOA, respectively; Agilent Technologies, Santa Clara, CA). qPCR reactions were performed in a final volume of 20 μl using 10 nM primers and the SYBR-Green mix (Roche Applied Science, Mannheim, Germany), and amplicons were subjected to either the ABI7500 or 7900 Fast Sequence Detection Systems (Life Technologies, Carlsbad, CA). Use of either the WT or mutant forward primer plus the common primer generated a 73-bp PCR product. The following PCR conditions were used: 10 min at 95°C, followed by 40 cycles of 15 sec at 95°C and 60 sec at 60°C.

Standard curves of amplicon levels were created by qPCR using serially-diluted pBS/wtRHOA or pBS/mutRHOA with WT or mutant primers, respectively.

Preparation of template plasmid DNA mixtures

pBS/mutRHOA was mixed with pBS/wtRHOA in 100, 10, 1.0, 0.1, 0.01 and 0% ratios. Overall DNA concentration was adjusted to 1.0 ng/well of a plate. All mixtures were then serially-diluted 1:10 for 4 cycles. qPCR was performed with these templates plus primers using conditions described above.

Patients and samples

Tumor samples were collected from 53 patients with AITL, 55 with PTCL-NOS, 19 with B-cell malignancies, 129 with myeloid malignancies, and 5 with another T-cell lymphoma (for a total of 261), according to WHO classification. Twenty-seven non-tumor samples, including bone marrow mononuclear cells and buccal cells from lymphoma patients, were also analyzed as controls. The Ethics Committee University of Tsukuba Hospital approved the protocol and consent procedure, according to which written informed consent was provided by the participants. Genomic DNA was extracted from 13 formalin-fixed/paraffin-

Table 1. Sequence of allele-specific primers used for this study.

Primer	Sequence
Forward (WT*[1])	ATTGTTGGTGATGGAGCCTGTGG
Forward (MUT*[2])	ATTGTTGGTGATGGAGCCTGTAT
Reverse (common)	ACACCTCTGGGAACTGGTCCT

*[1] WT, wild-type; *[2] MUT, mutant.
doi:10.1371/journal.pone.0109714.t001

Table 2. Analysis of genomic DNA samples.

Disease	Frozen amp*[1]	Frozen not-amp*[2]	PLP not-amp	FFPE not-amp	Total
AITL	14	10	19	10	53
PTCL-NOS	16	8	28	3	55
B-cell lymphoma	1	18			19
Myeloid malignancies	129				129
Other T-cell lymphomas		5			5
Control samples	27				27
Total	187	41	47	13	288

*[1]amp, amplified; *[2]not-amp, not-amplified.
doi:10.1371/journal.pone.0109714.t002

embedded (FFPE), 47 periodate/lysine/paraformaldehyde (PLP)-fixed, and 228 fresh frozen specimens, using an FFPE tissue kit (QIAGEN, Hilden, Germany) for FFPE and PLP samples and a Puregene DNA blood kit (QIAGEN) for fresh frozen specimens, according to manufacturer's instructions.

One hundred and one DNA samples were original, while 187 were whole genome-amplified by either GenomiPhi (GE, Fairfield, CT) or a RepliG mini kit (Qiagen) (Table 2). For DNA extracted from FFPE samples, we also prepared PCR amplicon with AmpliTaq Gold 360 (Life technologies) in a final volume of 20 μl with 20 ng genomic DNA, 5 nM primers (Table 3), 5 μl of AmpliTaq gold master mix, and 0.3 μl of 360 GC Enhancer. For this amplicon preparation, the following PCR conditions were used: one cycle of 15 min at 95°C, 4 min at 60°C, and 1 min at 72°C, next 35 cycles of 1 min at 95°C, 1 min at 60°C, and 1 min at 72°C, and finally 10 min at 72°C and kept at 4°C. Amplicons were purified using PCR purification kit (QIAGEN).

Each DNA sample was quantified using the Qubit dsDNA HS Assay kit and a Qubit fluorometer (Life Technologies, Carlsbad, CA). Extracted DNA samples were stored at −20°C until use.

For 108 of the total 288 genomic DNA samples, data sets for mutant allele frequencies obtained by deep sequencing using the MiSeq System (Illumina, San Diego, CA), which were used in our previous report [12], were reanalyzed.

qPCR of patient samples

qPCR reactions using duplicate patient samples were performed in a final volume of 20 μl with 50 ng of original or whole genome-amplified genomic DNA or 1.0×10^{-2} ng PCR-amplified DNA as a template, 10 nM primers, and the SYBR-Green mix (Roche, Basel, Switzerland) in conditions similar to those used for plasmid templates described above.

Levels of amplicons generated using either the WT or mutant primer, calculated with reference to respective standard curves, were designated [wt] and [mut], respectively.

Table 3. Primer sequences for making PCR amplicons of FFPE samples.

Primer	Sequence
Forward	GCCCCATGGTTACCAAAGCA
Reverse	GCTTTCCATCCACCTCGATA

doi:10.1371/journal.pone.0109714.t003

Statistical analysis

Statistical analysis was conducted using SPSS software (Japan International Business.

Machines Corporation, Tokyo). A P-value <0.05 was considered statistically significant.

Figure 2. Melting curve analysis. A. Melting curve constructed using WT allele-specific primers. B. Melting curve constructed using mutant allele-specific primer set.
doi:10.1371/journal.pone.0109714.g002

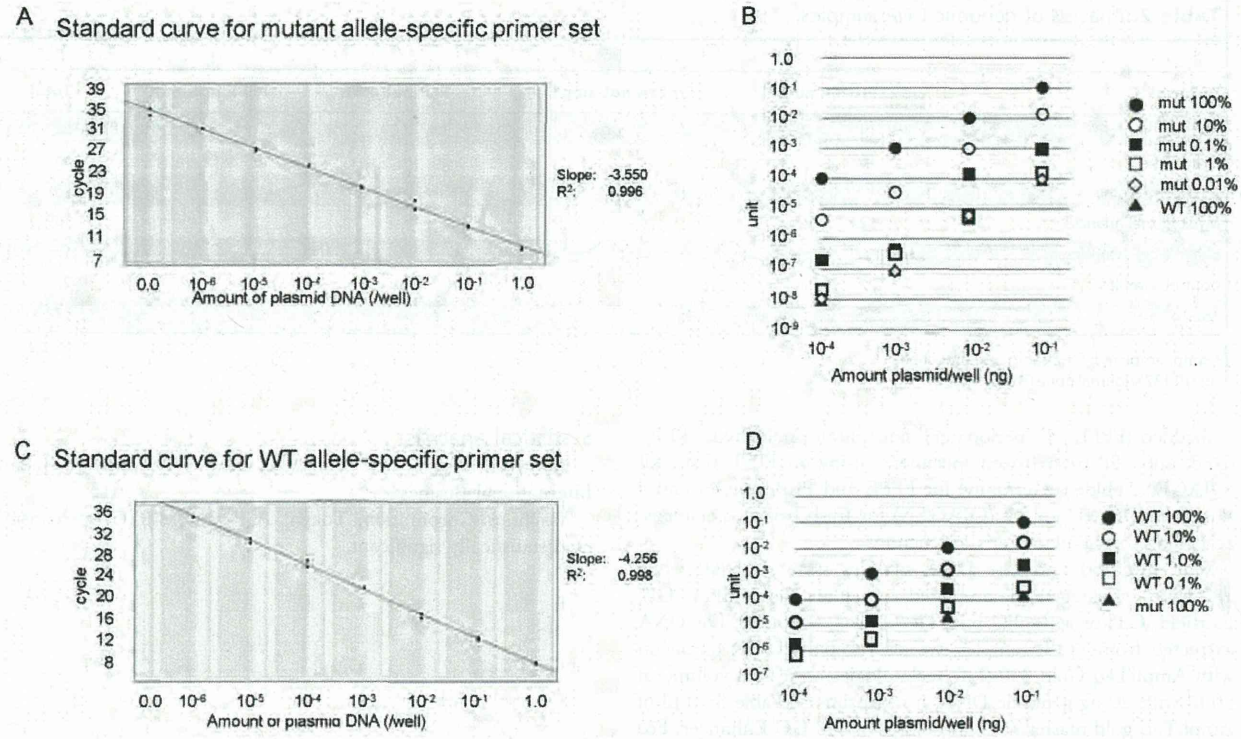

Figure 3. Standard curve showing linearity of quantitative allele-specific PCR. A standard curve was generated by serial dilution of WT or G17V cDNA that had been subcloned into pBluescript. A. Serial dilution of pBS/mutRHOA. Black dots correspond to 1.0×10^{-9}~1.0 unit of mutant plasmid (duplicate samples). The titration slope is −3.550 and R^2 is 0.996. B. pBS/mutRHOA was mixed with pBS/wtRHOA at 100%, 10%, 1.0%, 0.1%, 0.01% and 0%. Mix concentrations were adjusted to 1.0 ng/well and diluted 1:10 4 times for quantitative PCR analysis with allele-specific mutant primers. Horizonal axis indicates the amount of DNA per well. Vertical axis indicates unit for each sample. Black dot, MUT 100%; open dot, MUT 10%; square, MUT 1%; open square, MUT 0.1%; diamond, MUT 0.01%; triangle, MUT 0% (WT 100%) C. Serial dilution of pBS/wtRHOA. Black dots correspond to 1.0×10^{-6}~1.0 unit of WT cDNA (duplicate samples). The titration slope is −4.256, and R^2 is 0.998. D. pBS/wtRHOA was mixed with pBS/mutRHOA at 100%, 10%, 1.0%, 0.1%, 0.1% and 0%. Mix concentrations were adjusted to 1.0 ng/well and diluted 1:10 4 times for quantitative PCR analysis with WT allele-specific primers. Black dot, WT 100%; open dot, WT 10%; square, WT 1%; open square, WT 0.1%; triangle, WT 0% (MUT 100%).
doi:10.1371/journal.pone.0109714.g003

Results

Primer specificity

Melting curve analysis revealed that amplicons generated using either WT or mutant primers melted at 76.8°C or 75.3°C, respectively. Non-specific amplicons were not observed in either pBS/wtRHOA/WT primer or pBS/mutRHOA/mutant primer combinations (Figures 2A and 2B).

Linearity of amplicon generation

We then varied either the ratio of pBS/mutRHOA to pBS/wtRHOA or the concentration of total input DNA, and measured the amounts of PCR product generated using the mutant primer. Because we observed a nearly linear relationship between the amounts of generated amplicon and input DNA in the range of 10^4 (1–0.0001 ng DNA/well) at each ratio of pBS/mutRHOA to pBS/wtRHOA (Figure 3A), we defined the amount of amplicon derived from 100% pBS/mutRHOA template at 0.1 ng/well as 0.1 unit, and tested whether linearity was maintained with varying ratios of pBS/mutRHOA to pBS/wtRHOA. The template samples of 0.1 ng/well containing 10, 1, 0.1, and 0.01% pBS/mutRHOA were measured as 1.0×10^{-2} unit (C.I. (confidence interval), $0.8–1.3\times10^{-2}$; S.F. (scaling factor), 0.95–1.06), 1.2×10^{-3} unit (C.I., $0.8–1.6\times10^{-3}$; S.F., 0.96–1.07), 2.2×10^{-4} unit (C.I., $1.5–3.0\times10^{-4}$; S.F., 1.05–1.14), and 1.0×10^{-5} unit (C.I., $0.4–1.6\times10^{-5}$; S.F., 0.92–1.04), indicative of linearity in the range of 10^4 (100–0.01%). Taken together, linearity was maintained in the range of 10^9 (Figures 3A and 3B).

Similarly, when we assessed the WT primer using various ratios of pBS/wtRHOA to pBS/mutRHOA and concentrations of input DNA, linearity between the amounts of amplicon and template were maintained between 100–0.1% (a range of 10^3) and 1–0.001 ng DNA/well (a range of 10^3). This analysis indicated a total dynamic range of 10^6 (Figures 3C and 3D).

qAS-PCR of T-cell lymphoma samples

qAS-PCR with 50 ng of genomic DNA was performed using 106 AITL and PTCL-NOS samples including 11 FFPE samples. The [wt] and [mut] values were distributed between 7.9×10^{-5} and 1.8×10^{-1} units, and 2.0×10^{-7} and 7.6×10^{-2} units, respectively. Nevertheless, it was not possible to use absolute values of [mut] for levels of G17V *RHOA* alleles, due to variation in DNA quality. Therefore, we undertook relative measures to assess G17V *RHOA* allele frequency. To do so, we calculated a [mut]/([wt]+[mut]) value and compared it with mutant variant allele frequencies determined by MiSeq. [mut]/([wt]+[mut]) values were distributed between 3.2×10^{-4} and 3.0×10^{-1}. Among samples judged to harbor a G17V *RHOA* mutation by deep sequencing using the MiSeq System (cut-off level, 0.02), which was defined in previous paper [12], [mut]/([wt]+[mut]) values of DNA

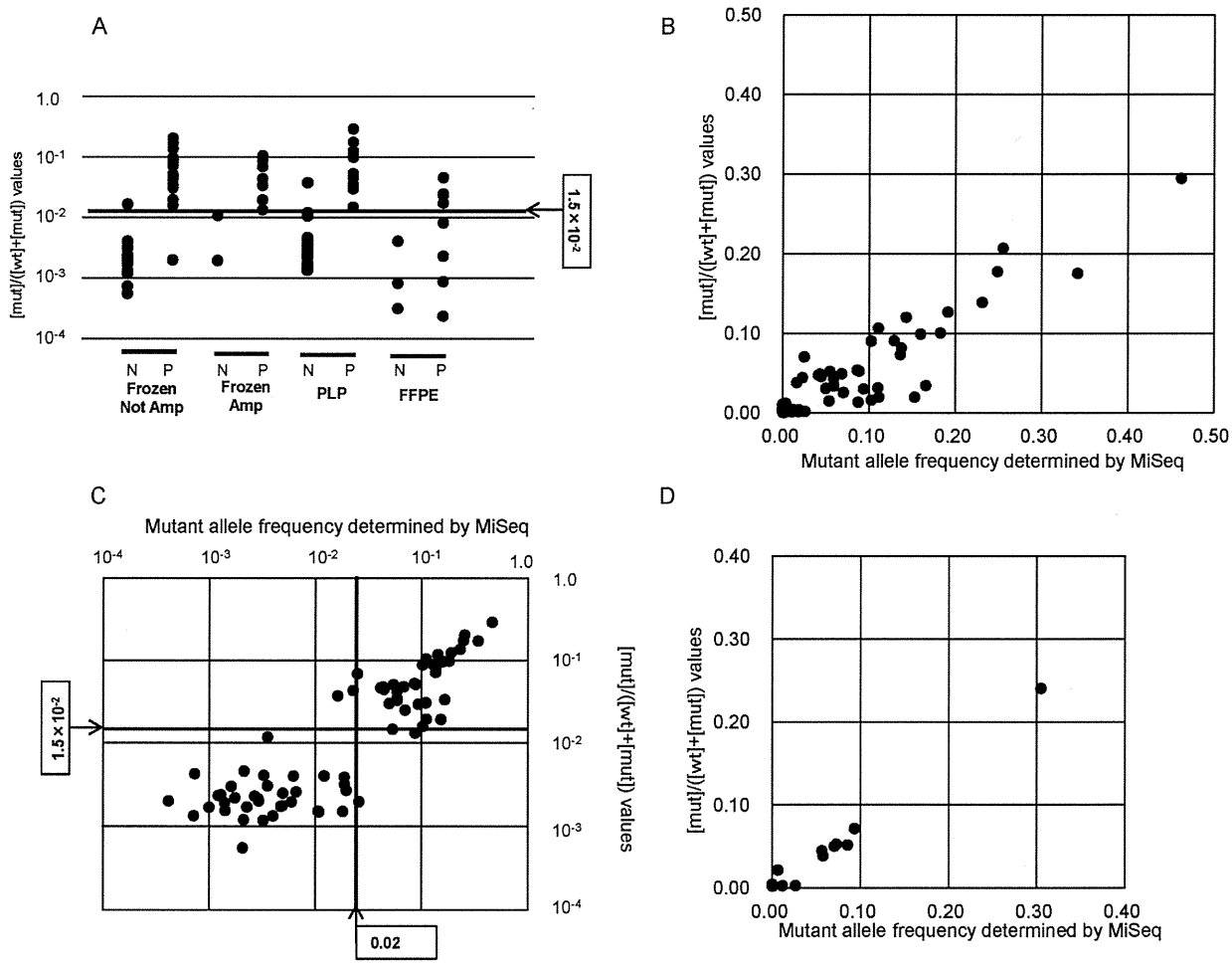

Figure 4. qAS-PCR of AITL and PTCL-NOS samples. A, Shown are [mut]/([wt]+[mut]) values for each sample. N, mutation negative determined by MiSeq; P, mutation positive determined by MiSeq; Amp, amplified; PLP, periodate/lysine/paraformaldehyde-fixed; FFPE, formalin-fixed/paraffin-embedded. B, Comparison of [mut]/([wt]+[mut]) values by qAS-PCR and mutant allele frequencies as determined by MiSeq for 95 original or whole genome-amplified DNA samples, including 43 AITL and 52 PTCL-NOS. Cut-off values were determined as 1.5×10^{-2} for [mut]/([wt]+[mut]) by qAS-PCR and as 0.02 for mutant allele frequencies as determined by MiSeq. C, Comparison of [mut]/([wt]+[mut]) values by qAS-PCR and mutant allele frequencies as determined by MiSeq for 95 DNA samples in a log scales. D, Comparison of [mut]/([wt]+[mut]) values by qAS-PCR and mutant allele frequencies as determined by MiSeq for 13 FFPE PCR-amplicon samples.
doi:10.1371/journal.pone.0109714.g004

from MiSeq-positive FFPE samples were significantly lower than those from other MiSeq-positive samples (Miseq-positive FFPE vs MiSeq-positive other samples; 1.56×10^{-2} vs. 9.38×10^{-2}, $p<0.05$, Student's t-test) (Figure 4A). Four out of all 8 MiSeq-positive FFPE samples were negative by qAS-PCR. Therefore, we excluded FFPE samples and analyzed data from 95 DNA samples that had been purified from PLP-fixed or frozen tissues.

When [mut]/([wt]+[mut]) values were compared with mutant variant allele frequencies determined by MiSeq, the rank correlation coefficient was 0.785 (Spearman's correlation $P<0.001$) (Figure 4B and C). Among the 95 samples analyzed, 38 (29 AITL and 9 PTCL-NOS) were judged positive and 57 (14 AITL and 43 PTCL-NOS) were judged negative by MiSeq. By comparison, when the cut-off level for [mut]/([wt]+[mut]) values was set at 1.5×10^{-2}, according to ROC curve (Supplemental Figure 1), 38 cases were judged positive for the G17V *RHOA* mutation, including 29 AITL and 9 PTCL-NOS. Overall, 91 of 95 specimens showed concordant results using both methods, while 4 cases showed discordant results (Figure 4B and C). If we assume that data generated by MiSeq is accurate, then the sensitivity and specificity of qAS-PCR were as high as 94.7% and 96.5%, respectively. Positive and negative concordance rates of the two methods were 94.7% and 96.5%, respectively (Table 4, Table S1 in File S1).

The four cases showing discordant results provided us with an insight into the comparison between MiSeq and aAS-PCR. Two samples were positive only based on MiSeq, and two were positive only by qAS-PCR. When we performed HISEQ2000 sequencing [12] for all these four samples, we observed $\geqq 0.02$ mutation allele frequencies in two samples. One had been deemed positive only by qAS-PCR and the other only by MiSeq. The other two samples showed <0.02 mutation allele frequencies by HISEQ2000. One of them was judged as negative only by qAS-PCR and the other only by MiSeq. Overall, accuracy with qAS-PCR and MiSeq was comparable.

Table 4. Correlation between qAS-PCR and MiSeq.

Method	Standard	Samples		N*[1]	RCC*[2]	Sensitivity	Specificity	PPV*[3]	NPV*[4]
qAS-PCR	MiSeq	AITL and PTCL-NOS	non- FFPE	all	95	0.785	94.7	96.5	94.7	96.5
				original	66	0.735	100.0	95.5	91.7	100.0
				WGA*[5]	29	0.822	87.5	100.0	100	86.7
			FFPE *[6]		13	0.919	87.5	80.0	87.5	80.0

*[1]N, number; *[2]RCC, rank correlation coefficient; *[3]PPV, positive predictive value; *[4]NPV, negative predictive value, *[5]WGA, whole-genome amplification. *[6]FFPE, formalin-fixed/paraffin-embedded.

doi:10.1371/journal.pone.0109714.t004

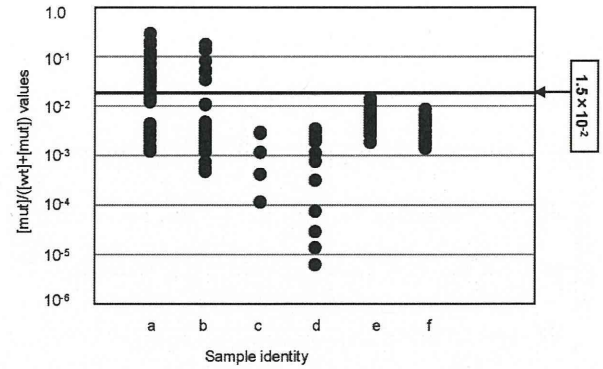

Figure 5. qAS-PCR for 275 tumor and control samples. qAS-PCR was performed for tumor samples, including 43 AITL (a), 52 PTCL-NOS (b), 5 T-cell lymphoma other than AITL and PTCL-NOS (c), 19 B-cell lymphomas (d), 129 myeloid malignancies (e) and 27 control samples (f).

doi:10.1371/journal.pone.0109714.g005

The qAS-PCR method using 50 ng of whole-genome-amplified DNA did not provide a robust correlation with the Miseq data for FFPE samples. The main reason was likely to be fragmentation of genomic DNA. To overcome this limitation, DNA prepared from the 13 FFPE samples was pre-amplified by PCR prior to performing qAS-PCR. Sensitivity and specificity for FFPE samples using amplicon was 87.5% and 80.0%, respectively, based on the mutation allele frequencies determined by MiSeq. (Figure 4D, Table S2 in File S1). Therefore, even for FFPE samples, the qAS-PCR method could robustly estimate the G17V RHOA mutation allele frequencies.

Effect of whole-genome amplification for qAS-PCR

When we divided the 95 samples into original DNA and whole-genome-amplified DNA cohort, sensitivity and specificity were 100% and 95.5% for original DNA cohort, and 87.5% and 100% for whole-genome-amplified DNA cohort, respectively (Supplemental Figure 2A-D, Table S3A and B in File S1).

In order to determine whether amplification influences the evaluation of mutation allele frequency by qAS-PCR, we compared the data for 15 pairs of original and whole-genome-amplified samples. Fourteen out of 15 pairs showed concordant results with each other (Table S3C and D in File S1, Figure S2E in File S1). One sample, which was judged positive by MiSeq, showed discordant results by qAS-PCR; positive for the original DNA and negative for the whole-genome-amplified DNA. As a summary, with some limitations, whole-genome-amplified DNA could provide robust results in most cases.

qAS-PCR for myeloid, B-cell and other T-cell malignancies

We performed qAS-PCR for buccal cells and non-tumor samples including bone marrow cells without lymphoma infiltration obtained from lymphoma patients, and confirmed that the qAS-PCR values were below the cut-off level in all samples. Then, we applied qAS-PCR for 153 tumor samples other than AITL and PTCL-NOS, including 129 myeloid, 19 B-cell, and 5 T-cell malignancies. Sanger sequencing also showed no mutant signals for any of these samples. All qAS-PCR values calculated using these samples were below the cut-off level (Figure 5).